

NUMERICAL INVESTIGATION OF THE DESTABILIZATION OF SUPERCRITICAL ROUND TURBULENT JETS USING LARGE-EDDY SIMULATION

T. Schmitt¹, A. Ruiz¹, L. Selle^{2,3}, B. Cuenot¹

¹*CERFACS, 42 Avenue G. Coriolis, 31057 Toulouse cedex, France*

²*Université de Toulouse; INPT, UPS; IMFT (Institut de Mécanique des Fluides de Toulouse); Allée Camille Soula, F-31400 Toulouse, France*

³*CNRS; IMFT; F-31400 Toulouse, France*

October 15, 2010

Abstract

In rocket engines, dense oxygen is injected in a high pressure environment, above its critical pressure. Oxygen temperature varies from a subcritical value at injection to a supercritical value in the burnt gases. Both the Vulcain 2 engine and the Space Shuttle main engine uses this injection mode. Thermodynamics, mixing and transport properties are no longer those of a perfect-gas mixture. The present study uses the Large Eddy Simulation code AVBP, developed at CERFACS to simulate such jets. Dense fluid flows are modelled by the use of a cubic equation of state, in conjunction with appropriate viscosity and thermal conductivity coefficients. A nitrogen round jet at supercritical pressure injected in a gaseous reservoir is simulated. Two cases are considered, one experiencing a transcritical injection (high-density injection), while the other one is injected at supercritical temperature (low-density injection). Mixing efficiency is studied and the stabilizing effect of the density gradients is identified. Results are in good agreement with available measurements. The funding for this research is provided by Snecma and CNES.

In rocket engines, dense oxygen is injected in a high pressure environment, above its critical pressure. Oxygen temperature varies from a subcritical value at injection to a supercritical value in the burnt gases. Both the Vulcain 2 engine and the Space Shuttle main engine uses this injection mode. In such conditions, fluid behavior may strongly differ from that of a perfect gas [1, 2]. In order to gain insight into the physics of high-pressure flows in complex configurations, the development of a CFD code for

predicting the flow features is of great interest and of great need, especially for long lasting development cycles as in the aerospace industry. For this reason Snecma, which is the prime contractor for European launcher Ariane 5 cryogenic propulsion systems and CNES (Centre National d'Etudes Spatiales), which is the government agency responsible for shaping and implementing France's space policy in Europe, have launched a program on the development of LES for supercritical combustion.

High-pressure cryogenic round jets were experimentally studied by AFRL (Air Force Research Laboratory) and DLR (Deutsches Zentrum für Luft- und Raumfahrt) [3, 4, 5, 6, 7, 8, 9, 10, 11, 12]. Both laboratories noticed a strong impact of pressure on the jet topology. Indeed, as pressure reaches its critical value, the classical behavior of two-phase jets is no longer observed, and dense fluid is continuously dissolved in ambient gas, leading to the apparition of high density gradients between the dense cold jet and the ambient gas, with no evidence of droplet formation. Part of the DLR experimental results on cryogenic round jets has served as a test case, referenced as RCM-1, in the 2nd International Workshop on Rocket Combustion Modeling [13].

Supercritical fluid behavior was also studied numerically, in particular with Direct Numerical Simulation (DNS) of mixing layers, showing the role of density gradients on the global layer stability and turbulence characteristics [14]. Only few LESs have been performed under supercritical-pressure conditions. An extensive review of the non-reacting LESs up to 2006 can be found in Zong and Yang [15]. A single nitrogen round jet was studied by Zong [16, 17]. The stabilizing effect of the density gradient, and its role on turbulent energy redistribution along the mixing layer was identified. Zong and Yang [18] also simulated a coaxial injection of oxygen and methane while shear coaxial LOx/GH₂ jet flame at supercritical pressure was investigated by both Matsuyama [19] and Oefelein [20]. To the author's knowledge, the studies from Zong [16, 17], who simulated high-pressure round jets from AFRL experiments, are the only unstationary analysis of a 3D non-reactive cryogenic round jet at high Reynolds number. RCM-1 test case has been simulated using RANS approach by Branam and Mayer [9] and Cheng and Farmer [21]. The aim of the current study is to describe the destabilization processes for a nitrogen jet under supercritical conditions.

For a proper description of supercritical (SC) fluid dynamics, two major modifications must be made to the standard low-pressure Navier Stokes equations:

- An Equation Of State (EOS) that accounts for real-gas effects must be implemented.
- Transport models for mass and heat transfers must be modified.

The equation of state can be considered as the cornerstone of SC fluid modeling since it ensures the accuracy of the method in a quiescent fluid. Indeed, basic thermodynamic variables such as the density or the pressure dependence of the heat capacities are directly driven by the EOS. From a practical point of view, the equation of state must compromise between accuracy and computational cost, leading to cubic equations of state.

This paper is organized as follows : real-gas models are presented in Section 1, then

the flow configuration and the numerical setup of the present simulation is presented in Section 2. Finally results are discussed in Section 3.

1 REAL GAS MODEL

In this section, two key ingredients of the numerical simulation of supercritical flows are presented: the EOS and the model for transport phenomena. The Peng-Robinson equation of state [22] was chosen for this work and has been implemented in the AVBP LES solver [23]. For a single species, it reads:

$$P = \frac{\rho r T}{1 - b\rho} - \frac{\rho^2 a(T)}{1 + 2b\rho - b^2\rho^2} \quad (1)$$

where P is the pressure, T the temperature, ρ the density and $r = R/W$ with R being the universal gas constant and W the molar mass. The coefficients $a(T)$ and b are defined as:

$$a(T) = 0.457236 \frac{(rT_c)^2}{P_c} \left[1 + c \left(1 - \sqrt{\frac{T}{T_c}} \right) \right]^2 \quad (2)$$

$$b = 0.077796 \frac{rT_c}{P_c} \quad (3)$$

where P_c is the critical pressure, T_c the critical temperature and the additional parameter c is defined as a function of the acentric factor ω_{ac} [24] by:

$$c = 0.37464 + 1.54226 \omega_{ac} - 0.26992 \omega_{ac}^2 \quad (4)$$

with $\omega_{ac} = 0.0372$ for N₂

Equation 1 is then used for a consistent derivation of the pressure dependence of thermodynamic coefficients (heat capacities, speed of sound, etc.), similarly to the procedure used by Miller *et al.* [25], and the low-pressure reference is provided by the JANAF thermochemical tables [26]. The performance of this model for the present study is illustrated in Fig. 1 by comparing the density and the constant-pressure heat capacity C_p with data from the NIST database [27] at 40 bars and within the temperature range of the experimental conditions presented in Section 2.

The relative error is less than 3% for the density and 10% for the heat capacity, except near the pseudo-boiling line (c.f. Fig. 1 (b) around 130 K) where the error locally increases to 5% for the density and 20% for the heat capacity. The pseudo-boiling temperature T_{pb} is the temperature for which, at a given pressure, the constant-pressure heat capacity C_p reaches its maximum; it is the prolongation of the gas/liquid phase-change line [11].

Harstad and Bellan [28] proposed a formulation of transport phenomena under supercritical conditions consistent with kinetic theory at low-pressure. For the configuration considered in this work (c.f. Section 2), many simplifications can be made. Indeed, for

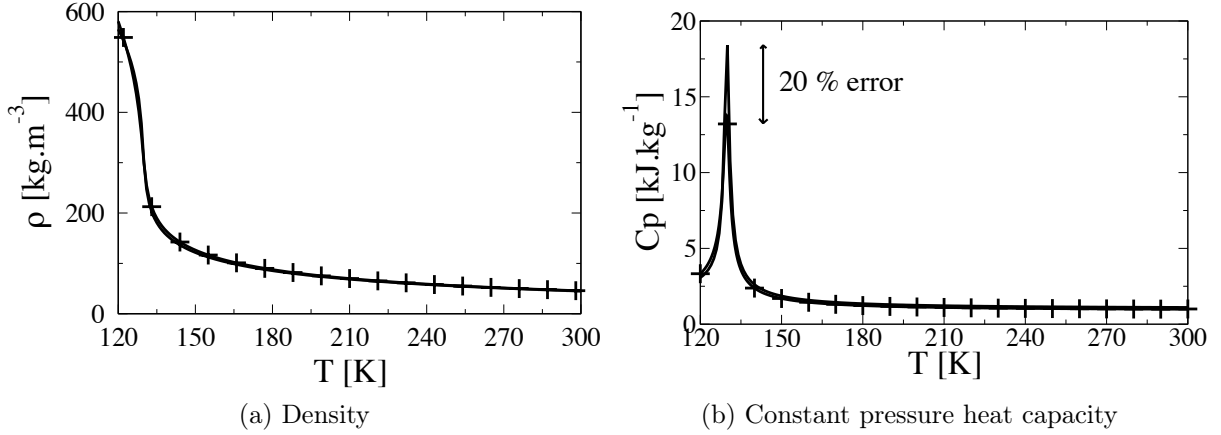


Figure 1: Validation of the EOS and thermodynamics for N2 at 40 bars ($P_{c_{N_2}} = 34 \text{ bars}$, $T_{c_{N_2}} = 126 \text{ K}$): — NIST database; —+— real-gas model, based on the PR EOS [22]

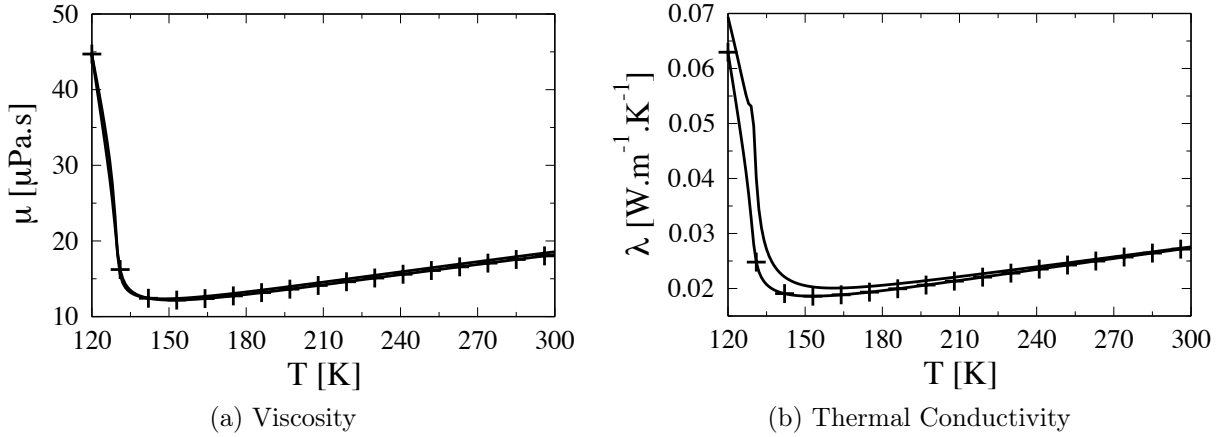


Figure 2: Validation of the transport coefficients : — NIST database; —+— Chung *et al.* [29]

single-species calculations, the only term that remains in the heat flux q_i is the classical Fickian contribution:

$$q_i = \lambda \frac{\partial T}{\partial x_i} \quad (5)$$

where λ is the thermal conductivity. The method proposed by Chung *et al.* [29] is used to compute the transport coefficients: the thermal conductivity and the dynamic viscosity μ . This method is based on the kinetic theory of gases, empirically corrected at high pressures. These coefficients compare favorably with the NIST database within the thermodynamic conditions of this study (Fig. 2), with a mean relative error of 3% for the thermal conductivity and 0.6% for the dynamic viscosity, over the 120K-300K temperature range. Altogether, this model provides a quantitative evaluation of thermodynamic variables over a wide range of pressure (not shown here) and temperature. Noteworthy, it naturally degenerates toward perfect-gas behavior when the pressure is decreased.

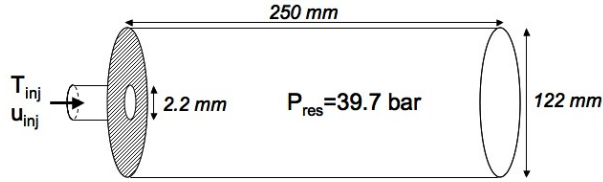


Figure 3: Sketch of the configuration

Case	T_{inj} [K]	u_{inj} [m/s]	T/T_{pb}	ρ_{inj}/ρ_{∞}	Re_{inj}
3	126.9	4.9	0.98	9.6	$1.7 \cdot 10^5$
4	137	5.4	1.06	3.7	$1.6 \cdot 10^5$

Table 1: Operating conditions for cases 3 and 4 of Mayer *et al.* [9, 10]

2 FLOW CONFIGURATION

The configuration for the numerical simulations is the experimental setup of Mayer *et al.* [9, 10]. It consists of a single round jet (diameter 2.2 mm) injected in a cylindrical chamber (diameter 122 mm) pressurized at 39.7 bar at a temperature of 298 K (Fig. 3). As the chamber diameter is 60 times larger than the injector diameter, the jet is believed to behave as a free jet.

2.1 Thermodynamic Conditions

Two cases with a different inlet temperature were computed and are presented in Table 1. The two cases are numbered according to Mayer *et al.* [9, 10].

Case 3 is a so-called «transcritical» injection: the injected fluid is evolving from a liquid-like state (high density) to a gas-like state (low density) after being heated up by the ambient warm gas. A large amount of energy is needed to change the jet temperature, as indicated in the C_p peak near the pseudo-boiling temperature T_{pb} in Fig. 4b.

The injection temperature of case 4 is very similar to case 3, however it is above the pseudo-boiling temperature ($T_{pb} = 129.5 K$ at 39.7 bar for nitrogen), which reduces the difference with a perfect-gas case. Hence, case 4 is merely qualified as «supercritical» injection in the following.

Because of the strong changes in dynamic viscosity near the pseudo-boiling temperature (Fig. 2a), the Reynolds numbers at injection for cases 3 and 4 are very close: $Re_{inj} \sim 160\,000$.

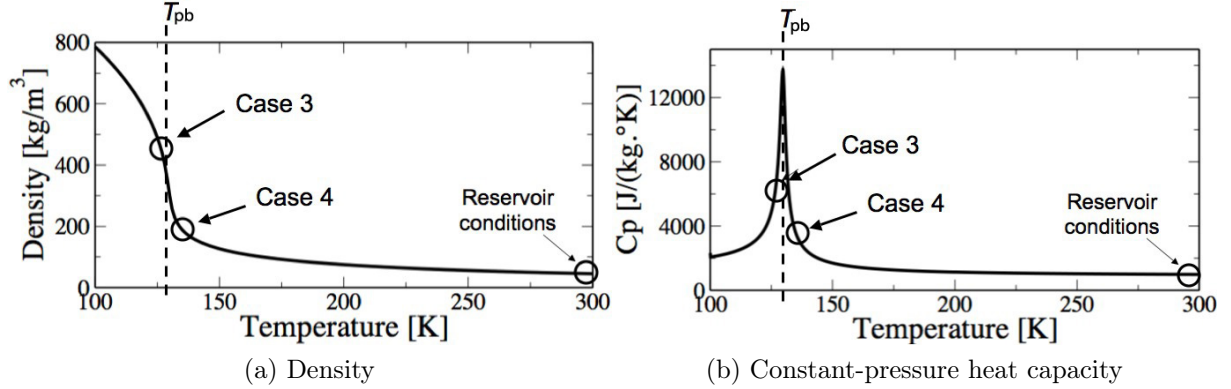
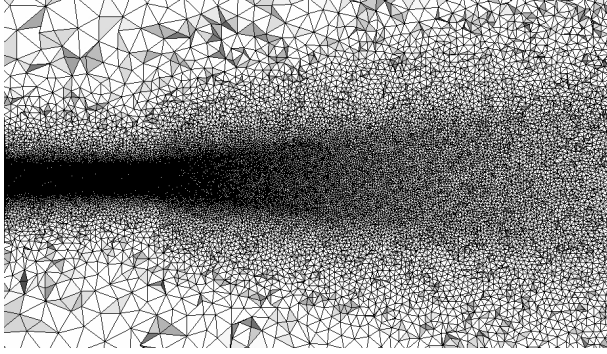


Figure 4: Injection conditions for case 3 and case 4

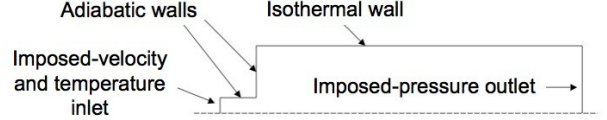
2.2 Numerical Setup: Mesh and Boundary Conditions

The computational domain used in the present 3D simulation corresponds to the experimental setup from Branam and Mayer [9]. A longitudinal cut of the mesh is displayed in Fig. 5a. The grid is finest near the injector, with a constant characteristic cell size of 0.1 mm over a distance of almost ten diameters. This zone is followed by a smoothly coarsening region. The mesh, which is the same for both cases, contains 950 000 points and 5 500 000 tetrahedra. The boundary conditions used in the present simulation are presented in Fig. 5b. The pressure in the reservoir is maintained by a non-reflecting outlet with a target pressure using the NSCBC technique [30] made consistent with the real-gas EOS [31]. The walls near the injector are treated as adiabatic while the reservoir walls are kept at a constant temperature of 298 K. The velocity and temperature are imposed at the inlet with turbulent perturbations prescribed by the procedure initially developed by Kraichnan [32, 33] and adapted to compressible flows [34] with an intensity of 2.5 % of the mean flow.

The simulation is achieved using the TTGC scheme [35]. This centered scheme is third order in time and space and has successfully been validated for both non-reacting and reacting flows [36]. Cryogenic jets at supercritical pressure are characterized by very steep density gradients which require specific numerical treatments. The steep density gradients are localized using a Jameson-like sensor [37] and artificial viscosity is added to the conservation equations in the regions indicated by this sensor. The highly non-linear thermodynamics requires a consistent treatment of artificial fluxes to avoid spurious noise generation [38].



(a) Longitudinal cut of the computational domain's mesh on a length of 30 injector diameters



(b) Boundary conditions

Figure 5: Numerical setup

3 RESULTS

First, the quality of the present LES is assessed using the criterion proposed by Pope [39], which is presented in Figure 6:

$$M = \frac{k_{sgs}}{k_{sgs} + k_{res}} \quad (6)$$

where k_{sgs} and k_{res} are the subgrid scale turbulent energy and the resolved kinetic turbulent energy, respectively. The following expressions are used:

$$k_{sgs} = \left(\frac{\nu_t}{0.1 * \delta} \right)^2 \quad (7)$$

$$k_{res} = (u_{rms}^2 + v_{rms}^2 + w_{rms}^2) / 2 \quad (8)$$

where ν_t , δ , u_{rms} , v_{rms} and w_{rms} are the kinematic turbulent viscosity, the cell size and the RMS values of the velocity components, respectively. The white line in Figure 6 is 40 diameter long and indicates that more than 95% of the velocity fluctuations are resolved in this region. The coarsening of the mesh beyond the latter region makes this criterion reach 80%. However, no results are analyzed there and the overall mesh quality is correct.

The centerline profile of density was experimentally measured by Mayer *et al.* [9, 10] using 2D Raman technique. These results are compared with the present numerical simulations in Fig. 7. For case 3, the computational results accurately predict the drop in centerline density despite a small (10%) overestimation near the injector, which could be due to the systematic error of the Raman technique in very-high-density regions [9, 10]. This overestimation does not come from a lack of precision of the PR EOS, since the density from the NIST database is 20 kg.m⁻³ higher than the density from the PR EOS, at the injection thermodynamic state. For case 4 however, experimental and numerical results differ notably. This could come from a small discrepancy between the simulation and the experiment injection temperature, which implies a very large discrepancy between injection densities, since the inlet thermodynamic state is very close to the pseudo-boiling point (cf. Fig. 4a). Finally, based on the centerline density profiles, one can evaluate the dense-core length x_{DC} , which is defined, in the present study, as the downstream

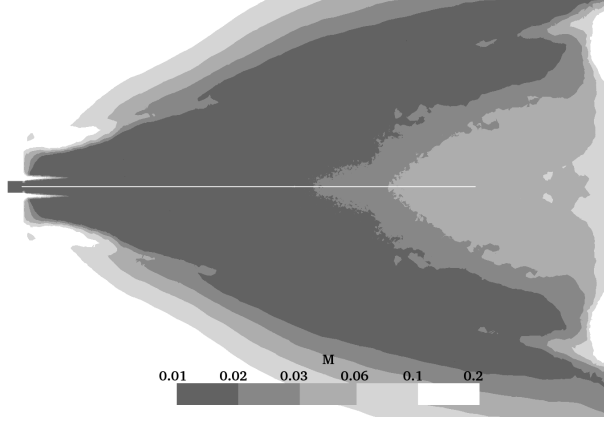


Figure 6: Estimation of the present LES quality, using the criterion from [39]

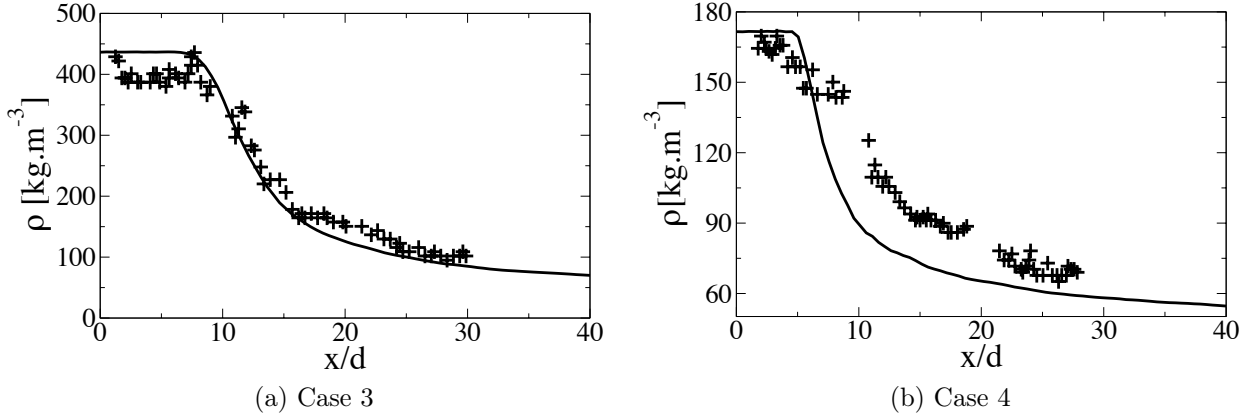


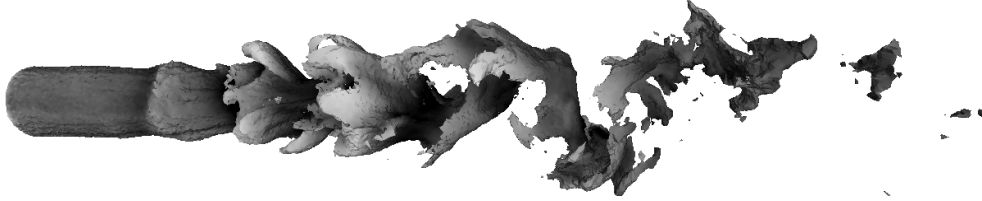
Figure 7: Comparison between experimental results and LES results of the centerline density in terms of normalized distance from the injector. — present LES ; + Mayer *et al.* [9, 10]

distance from the injector, where the density decreases below 99% of its injection value. It is found to be 7.9 diameters for case 3 and reduces to 5.1 diameters for case 4. The mixing efficiency is thus reduced for a transcritical injection, which is consistent with phenomenological studies of high-pressure jets [11].

In order to assess mixing efficiency, the initial destabilization of the dense-core and its transition to fully developed turbulence is studied. Fig. 9a shows the axial development of maximum radial velocity perturbations u'_r along the shear layer. The development of u'_r in the near-injector region is much faster in case 4 than in case 3. In case 4, it reaches 20% of u_{inj} at 2 diameters, while it reaches 10% of u_{inj} at 13 diameters in case 3. An exponential fit of the initial growth of the velocity perturbation is made in order to obtain a spatial amplification coefficient k_i ($u'_r = cst + exp(k_i x/d)$). In case 4, k_i is approximately four times as high as case 3. The growth of the velocity perturbations appears similar to the Kelvin-Helmholtz instability and shows the stabilizing effect of the density gradient.



(a) Case 3



(b) Case 4

Figure 8: Isosurface at $\rho^+ = 0.5$ colored by velocity magnitude

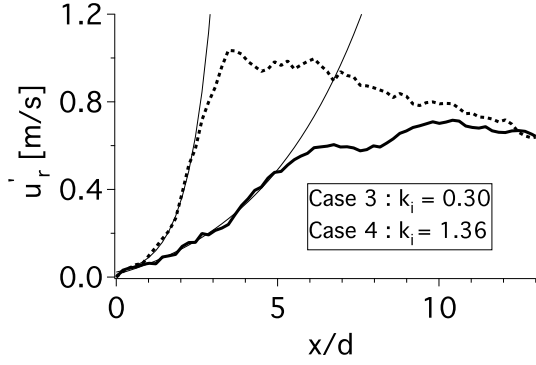
The effects of these velocity perturbations on the «dense fluid» is now investigated. The non-dimensional density ρ^+ is introduced:

$$\rho^+ = \frac{\rho - \rho_\infty}{\rho_{inj} - \rho_\infty} \quad (9)$$

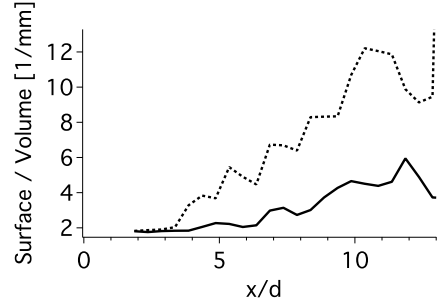
When $\rho^+ = 1$, the fluid has the injection density. When $\rho^+ = 0$, it has the reservoir density. An isosurface at $\rho^+ = 0.5$ colored by velocity magnitude (the darker, the higher velocity) is shown in Fig. 8, and the inner volume delimited by this isosurface is here called the «dense fluid». In case 3, the dense fluid is wrinkled by weak hydrodynamic instabilities and progressively disappears in the reservoir, whereas in case 4, the dense fluid bursts at a few diameters downstream of the injector, similarly to a gaseous jet disintegration. This is consistent with the radial velocity perturbation profiles shown in Fig. 9a. The wrinkling of the dense fluid is then assessed isolating one-diameter-long slices of the isosurfaces shown in Fig 8 and computing the surface to volume ratio of these slices. The instantaneous longitudinal evolution of the dense-fluid wrinkling is plotted in Fig. 9b. The wrinkling of the transcritical dense fluid is much lower than the supercritical one, which reduces the exchange surface between warm and cold fluid, therefore reducing heat transfer. Together with the C_p peak mentioned in Section 2.1, this extends the transcritical dense-core length.

In order to identify the phenomena responsible for the increase of velocity perturbations, the enstrophy ω^2 balance equation is analysed

$$\frac{D(\omega^2)}{Dt} = \underbrace{2\underline{\omega} \cdot (\underline{\omega} \cdot \underline{\nabla}) \underline{u}}_{Stretching} - \underbrace{2(\underline{\nabla} \cdot \underline{u}) \omega^2}_{Dilatation} - \underbrace{2\underline{\omega} \cdot \frac{\underline{\nabla} \rho \times \underline{\nabla} P}{\rho^2}}_{Baroclinic\ torque} + \underbrace{2\underline{\omega} \cdot \underline{\nabla} \times \left(\frac{1}{\rho} \underline{\nabla} \cdot \underline{\tau} \right)}_{Dissipation} \quad (10)$$



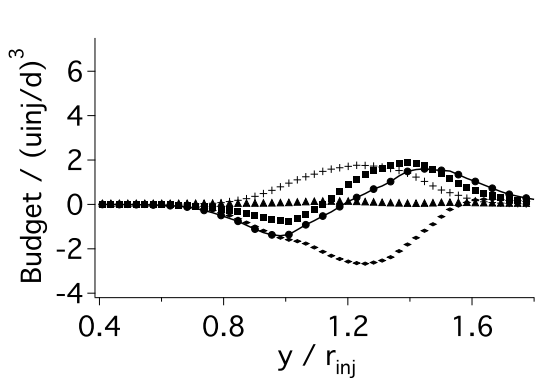
(a) Development of maximum radial velocity perturbations along the shear layer. — Case 3; Case 4; — exponential fits



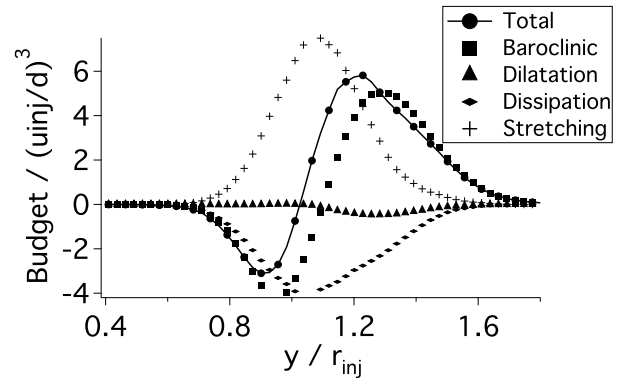
(b) Instantaneous wrinkling of the dense core. — Case 3; Case 4

Figure 9: Mixing efficiencies

where $\underline{\omega} = \nabla \times \underline{U}$, \underline{U} is the velocity and $\underline{\tau}$ is the viscous stress tensor. The average non-dimensional source terms of the enstrophy equation are plotted in Fig. 10 for both cases. The radial profiles are taken at $x/x_{DC} = 0.5$ in order to get information about the dense-core destabilization. As vortex stretching is approximately compensated by viscous dissipation, the sum of the all the source terms in Eq. 10 closely follows the profile of the baroclinic torque in both cases, showing that it is both responsible for the damping and the enhancement of the hydrodynamic instabilities in the dense fluid and the light fluid, respectively. Similar observations are made by Zong *et al.* [17] using LES and O’kongo *et al.* [40] using DNS. It appears that only the absolute value of the source terms are changed between case 3 and case 4 while their relative importance are approximately the same.



(a) Case 3, axial distance = 4 diameters



(b) Case 4, axial distance = 2.6 diameters

Figure 10: Enstrophy source terms in the transition zone of the two jets

4 CONCLUSION

Two simulations of supercritical round jets, representative of rocket injection thermodynamic conditions, has been successfully undertaken with the LES code AVBP, using the Peng-Robinson equation of state and appropriate transport coefficients.

Mean centerline density profiles have been obtained and compared with the experimental results of Mayer *et. al* [9, 10]. The results for the transcritical injection case (case 3, which has the most real-gas effects) show very good agreement with experimental measurements, with the correct decrease of the centerline density and the correct dense-core length, whereas unexpected discrepancies exist for the supercritical injection case (case 4). The transcritical dense core is longer than the supercritical one, which is in qualitative agreement with other high-pressure experimental results [11].

The spatial amplification of the radial velocity perturbations along the shear layer have been computed and the initial growth rate of these perturbations is approximately four times smaller in the transcritical case than in the supercritical case. The effects of these hydrodynamic perturbations on heat transfer has been identified through the evaluation of the «dense fluid» wrinkling, which is less intense in case 3 than in case 4. Hence, the extent of the transcritical dense core is not only due to the pseudo-phase change process but also to the reduced heat transfer induced by lower wrinkling.

Finally, the amplification mechanisms of the hydrodynamic perturbations have been studied through the evaluation of the enstrophy equation source terms and it has been shown that the driving phenomena is the baroclinic torque which damps perturbations in the dense fluid while enhancing them in the light fluid.

References

- [1] J. Hirschfelder, C. Curtis, and B. Bird. *Molecular Theory of Gases and Liquids*. John Wiley & Sons, 1954 edition, 1954.
- [2] B. E. Poling, J. M. Prausnitz, and J. P. O’Connell. *The properties of gases and liquids*. McGraw-Hill, 5th edition, 2001.
- [3] W. Mayer, A. Schik, C. Schweitzer, and M. Schaffler. Injection and mixing processes in high pressure LOX/GH2 rocket combustors, AIAA Paper No. 96-2620. 32nd AIAA/ASME/SAE/ASEE Joint Propulsion Conference & Exhibit, Lake Buena Vista, Florida, 1996.
- [4] W. Mayer and H. Tamura. Propellant injection in a liquid oxygen/gaseous hydrogen rocket engine. *J. Prop. Power* , 12(6):1137–1147, November-December 1996.
- [5] W. Mayer, A. Schik, B. Vielle, C. Chaveau, I. Gökalp, and D. Talley. Atomization and breakup of cryogenic propellants under high pressure subcritical and supercritical conditions. *J. Prop. Power* , 14(5):835–842, 1998.

- [6] W. Mayer, A. Ivancic, A. Schik, and U. Hornung. Propellant atomization in LOX/GH2 rocket combustors. *AIAA Paper*, pages 98–3685, 1998.
- [7] M. Oswald. Supercritical nitrogen free jet investigated by spontaneous raman scattering. *Experiments in Fluids*, 27:497–506, 1999.
- [8] B. Chehroudi, D. Talley, and E. Coy. Visual characteristics and initial growth rate of round cryogenic jets at subcritical and supercritical pressures. *Physics of Fluids*, 14(2):850–861, february 2002.
- [9] R. Branam and W. Mayer. Characterisation of cryogenic injection at supercritical pressure. *J. Prop. Power* , 19(3):342–355, May-June 2003.
- [10] W. Mayer, J. Telaar, R. Branam, G. Schneider, and J. Hussong. Raman measurements of cryogenic injection at supercritical pressure. *Heat and Mass Transfer*, 39:709–719, 2003.
- [11] M. Oswald, J. J. Smith, R. Branam, J. Hussong, A. Schik, B. Chehroudi, and D. Talley. Injection of fluids into supercritical environments. *Combust. Sci. Tech.* , 178:49–100, 2006.
- [12] W.O.H. Mayer and J.J. Smitht. Fundamentals of supercritical mixing and combustion of cryogenic propellants. *Liquid rocket thrust chambers: aspects of modeling, analysis, and design*, page 339, 2004.
- [13] J. Telaar, G. Schneider, J. Hussong, and W. Mayer. Cryogenic jet injection: Description of test case RCM 1. In *Proceedings 2nd International Workshop on Rocket Combustion Modeling, Lampoldshausen, Germany*, 2001.
- [14] J. Bellan. Theory, modeling and analysis of turbulent supercritical mixing. *Combust. Sci. Tech.* , 178:253–281, 2006.
- [15] N. Zong and V. Yang. Cryogenic fluid jets and mixing layers in transcritical and supercritical environments. *Combust. Sci. Tech.* , 178:193–227, 2006.
- [16] Nan Zong, Hua Meng, Shih-Yang Hsieh, and Vigor Yang. A numerical study of cryogenic fluid injection and mixing under supercritical conditions. *Physics of Fluids*, 16:4248–4261, December 2004.
- [17] N. Zong. Modeling and simulation of cryogenic fluid injection and mixing dynamics under supercritical conditions. *PhD thesis, Department of Mechanical and Nuclear Engineering, Pennsylvania State University*, 2005.
- [18] N. Zong and V. Yang. A numerical study of high-pressure oxygen/methane mixing and combustion of a shear coaxial injector. In *AIAA Paper*, 2005.
- [19] S. Matsuyama, J. Shinjo, Y. Mizobuchi, and S. Ogawa. A numerical investigation on shear coaxial lox/gh2 jet flame at supercritical pressure. In *44th AIAA Aerospace Sciences Meeting and Exhibit, Reno, Nevada*, 2006.

- [20] J.C. Oefelein. Thermophysical characteristics of shear-coaxial LOX-H₂ flames at supercritical pressure. *Proceedings of the Combustion Institute*, 30(2):2929–2937, 2005.
- [21] G.C. Cheng and R. Farmer. Real fluid modeling of multiphase flows in liquid rocket engine combustors. *J. Prop. Power*, 22(6):1373, 2006.
- [22] D. Y. Peng and D. B. Robinson. A new two-constant equation of state. *Ind. Eng. Chem., Fundam.*, 15(1):59–64, 1976.
- [23] T. Schönfeld and M. Rudgyard. Steady and unsteady flows simulations using the hybrid flow solver avbp. *AIAA Journal*, 37(11):1378–1385, 1999.
- [24] K.S. Pitzer, D.Z. Lippmann, RF Curl Jr, C.M. Huggins, and D.E. Petersen. The Volumetric and Thermodynamic Properties of Fluids. II. Compressibility Factor, Vapor Pressure and Entropy of Vaporization1. *Journal of the American Chemical Society*, 77(13):3433–3440, 1955.
- [25] Richard S. Miller, Kenneth G. Harstad, and Josette Bellan. Direct numerical simulations of supercritical fluid mixing layers applied to heptane-nitrogen. *Journal of Fluid Mechanics*, 436:1–39, 2001.
- [26] *NIST-JANAF Thermochemical Tables*. National Institute of Standards and Technology, 1998.
- [27] EW Lemmon, MO McLinden, and DG Friend. Thermophysical properties of fluid systems. *NIST chemistry webbook, NIST standard reference database*, 69, 2009.
- [28] J. Bellan K. Harstad. An all-pressure fluid drop model applied to a binary mixture: heptane in nitrogen. *International Journal of Multiphase Flow*, 26(10):1675–1706, October 2000.
- [29] T. H. Chung, M. Ajlan, L. L. Lee, and K. E. Starling. Generalized multiparameter correlation for nonpolar and polar fluid transport properties. *Industrial and Engineering Chemistry Research*, 27(4):671–679, 1988.
- [30] T. Poinso and S. Lele. Boundary conditions for direct simulations of compressible viscous flows. *J. Comput. Phys.*, 101(1):104–129, 1992.
- [31] N. Okong’o and J. Bellan. Consistent boundary conditions for multicomponent real gas mixtures based on characteristic waves. *J. Comput. Phys.*, 176:330–344, 2002.
- [32] R.H. Kraichnan. Diffusion by a random velocity field. *Phys. Fluids*, 13:22–31, 1970.
- [33] A. Smirnov, S. Shi, and I. Celik. Random flow generation technique for large eddy simulations and particle-dynamics modeling. *Trans. ASME. J. Fluids Eng.*, 123:359–371, 2001.

- [34] N. Guezennec and T. Poinso. Acoustically nonreflecting and reflecting boundary conditions for vorticity injection in compressible solvers. *AIAA Journal* , 47:1709–1722, 2009.
- [35] O. Colin and M. Rudgyard. Development of high-order taylor-galerkin schemes for unsteady calculations. *J. Comput. Phys.* , 162(2):338–371, 2000.
- [36] L. Selle, G. Lartigue, T. Poinso, R. Koch, K.-U. Schildmacher, W. Krebs, B. Prade, P. Kaufmann, and D. Veynante. Compressible large-eddy simulation of turbulent combustion in complex geometry on unstructured meshes. *c.f.* , 137(4):489–505, 2004.
- [37] A. Jameson, W. Schmidt, and E. Turkel. Numerical solution of the euler equations by finite volume methods using runge-kutta time stepping schemes. In AIAA paper 81-1259, editor, *14th Fluid and Plasma Dynamic Conference*, Palo Alto, 1981.
- [38] T. Schmitt, L. Selle, A. Ruiz, and B. Cuenot. Large-eddy simulation of supercritical-pressure round jets. *Am. Inst. Aeronaut. Astronaut. J.* , To be published.
- [39] S. B. Pope. Ten questions concerning the large-eddy simulation of turbulent flows. *New Journal of Physics*, 6:35, 2004.
- [40] N.A. Okong’o and J. Bellan. Direct numerical simulation of a transitional supercritical binary mixing layer: heptane and nitrogen. *J. Fluid Mech.* , 464:1–34, 2002.